Ferroic superglasses: Polar nanoregions in relaxor ferroelectric PMN versus CoFe superspins in a discontinuous multilayer

Wolfgang Kleemann*
Angewandte Physik, Universität Duisburg-Essen, D-47048 Duisburg, Germany

Jan Dec
Institute of Materials Science, University of Silesia, PL-40-007 Katowice, Poland

(Received 2 August 2016; revised manuscript received 20 October 2016; published 18 November 2016)

Superdipolar glass properties of polar nanoregions (PNRs) in relaxor ferroelectric $PbMg_{1/3}Nb_{2/3}O_3$ (PMN) are compared to those of ferromagnetic nanoparticles (FNPs) in the superspin glass $[Co_{80}Fe_{20}(0.9\,nm)/Al_2O_3(3\,nm)]_{10}$. Both the dynamic critical properties at $T > T_g$ and nonergodicity phenomena at $T < T_g$ are comparable, but this does not apply to their polydispersivity at $T \leqslant T_g$. Due to the quenched random size and position distribution of the FNP, the superspin glass exhibits standard Cole-Cole broadening of the spectrum of relaxation frequencies at all temperatures. Contrastingly, the relaxation spectrum of the PNRs in PMN is subject to a crossover from Lacroix-Béné to Cole-Davidson statistics on cooling toward T_g. Surprisingly, it becomes replaced by relaxation and creeplike domain-wall dynamics below T_g as a consequence of volume percolation of the PNR at T_g and formation of a ferroelectric microdomain state under the simultaneous control by quenched random electric fields and the softening ferroelectric F_{1u} lattice mode.

DOI: 10.1103/PhysRevB.94.174203

I. INTRODUCTION

The polar ground state of relaxor ferroelectrics ("relaxors" for short) such as the *B* cation disordered perovskite $PbMg_{1/3}Nb_{2/3}O_3$ (PMN) has been enigmatic ever since its discovery by Smolenskii and Agranovskaya [1]. In the early 1990s the discussion of the observed polar ordering at the nanoscale culminated in two competing models—the "dipole glass" [2] and the "domain state" of polar nanoregions (PNRs) under the constraint of quenched electric random fields (RFs) [3], respectively. Only recently have both ideas converged into the nonergodic ferroelectric cluster glass ground state emerging from the high-T PNR ensemble under random electrostatic interaction via a generic glass transition [4–6]. By virtue of their "superdipolar glass" ground state [7] relaxors have entered the materials family of mesoscopic "ferroic glasses" and are thus accepted to join spin cluster and strain glass [8], although some reservation still remains [9].

Indeed, not all the details of the properties of the superdipolar glass transition of relaxors have yet been presented. This paper is intended to fill this gap and to compare the glass transition of PMN to that of a classic superspin glass (SSG) consisting of ferromagnetic nanoparticles (FNPs) of $Co_{80}Fe_{20}$ being quench-condensed into an insulating matrix of alumina, Al_2O_3 [10]. Despite the clear dominance of frustrated (electric and magnetic, respectively) dipolar interactions, both systems still behave quite differently. While the FNP system is merely subject to frustrated (magnetic) dipolar interaction, the PNR system is primarily subjected to quenched random electric fields inherent in the charge disordered compound PMN [3,11]. First of all they are responsible for the PNR formation at high temperatures ($T_d \approx 600$ K). Thereafter they control the PNR growth and final percolation on cooling, and thus give rise to domainlike aggregation of PNRs at the glass transition ($T_g \approx 240$ K). These features make relaxors unique among all ferroic glasses.

II. EXPERIMENTAL PROCEDURE

Dielectric spectroscopy was studied on platelet-shaped (thickness ≈0.5 mm) samples with optically polished (001) faces cut from a flux-grown single crystal of PMN [3]. For the experiments the major faces were covered by electrodes of vacuum deposited copper with protective gold films. The complex dielectric susceptibility, $\chi = \chi' - i\chi''$, was measured with a Solartron 1260 impedance analyzer with 1296 dielectric interface at frequencies $10^{-3}\,\text{Hz} \leqslant f \leqslant 10^5\,\text{Hz}$. The amplitude of the ac probing field was $E_{ac} \approx 500\,\text{V/m}$. The temperature was stabilized to within ±0.005 K using a Lake Shore 340 temperature controller.

Corresponding magnetic ac susceptibility data were taken on a discontinuous magnetic metal-insulator multilayer (DMIM) of $[Co_{80}Fe_{20}(t_n)/Al_2O_3(3\,nm)]_{10}$ prepared by Xe ion-beam sputtering on glass substrates [12]. Up to a nominal thickness $t_n = 1.8$ nm nonpercolating discontinuous distributions of immiscible CoFe alloy clusters ("superspins") embedded within adjacent alumina layers are found. Figure 1(a) shows a transmission electron micrograph (TEM) of the irregular cluster (dark dots) distribution with partial hexagonal short-range ordering (white contours indicated) in a bilayer with $t_n = 0.9$ nm [10]. Their near Gaussian size distribution is shown in Fig. 1(b). The complex magnetic susceptibility, $\chi = \chi' - i\chi''$, was measured at room temperature with a Quantum Design MPMS-5S superconducting quantum interference device (SQUID) magnetometer at frequencies $10^{-2}\,\text{Hz} \leqslant f \leqslant 10^3\,\text{Hz}$ and an amplitude $\mu_0 H_{ac} = 50\,\mu\text{T}$ [12].

*Author to whom correspondence should be addressed: wolfgang.kleemann@uni-due.de

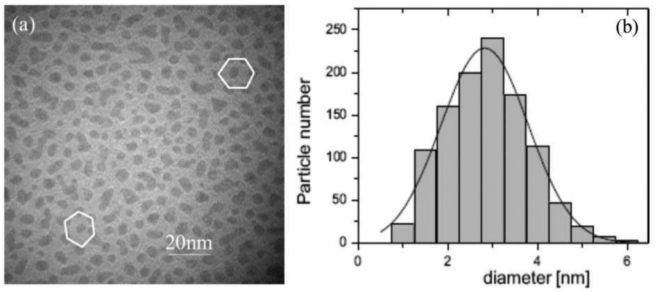

FIG. 1. (a) TEM top view micrograph of $Co_{80}Fe_{20}(0.9\,nm)/Al_2O_3(3\,nm)$ bilayer. (b) CoFe particle size distribution. Reproduced with permission from [10] via *CCC Rights Link*.

III. DYNAMIC SUPERGLASS CRITICALITY

Figure 2 shows the temperature dependence of the susceptibility components, χ' and χ'' vs T, of PMN for frequencies $10^{-3}\,\text{Hz} \leqslant f \leqslant 10^{5}\,\text{Hz}$ in decadic order at temperatures $197 \leq T \leq 297$ K. The $\chi'(T)$ curves reveal extremely broad peak widths, full width at half maximum (FWHM) ≥ 50 K, monotonic increase of their heights with decreasing f, and simultaneous low-T shifts of their peak positions, T_m. Qualitatively the same features are met in the $\chi'(T)$ curves of $[Co_{80}Fe_{20}(0.9\,nm)/Al_2O_3(3\,nm)]_{10}$ (Fig. 3) for frequencies $10^{-2} \leqslant f \leqslant 10^{0}$ Hz, and temperatures $30 \leq T \leq 90$ K [12].

As known from the theory of dipolar [13] and spin glasses [14] the (static) glass temperature is pinpointed by the divergence of the characteristic relaxation time $\tau = (2\pi f)^{-1}$ related to the peak temperatures $T_m(f)$ of χ' via the power law of critical dynamics [15],

$$\tau(T_m) = \tau_0(T_m/T_g - 1)^{-z\nu}. \tag{1}$$

For PMN a best fit of the asymptotic lowest frequency data within $10^{-3} \leqslant f \leqslant 2 \times 10^{-2}$ Hz (Fig. 4: right dataset; arrows), yields the (static) glass temperature $T_g = (238.8 \pm 1.1)$K and the relatively large attempt time $\tau_0 = (4.3 \pm 0.1) \times 10^{-10}$ s in accordance with the mesoscopic size of the PNR in PMN in the critical regime [16]. The dynamic critical exponent $z\nu = 7.9 \pm 0.3$ agrees within errors with that of the three-dimensional (3D) magnetic dipolar glass $LiHo_{0.045}Y_{0.955}F_4$, $z\nu = 7.8 \pm 0.2$ [17].

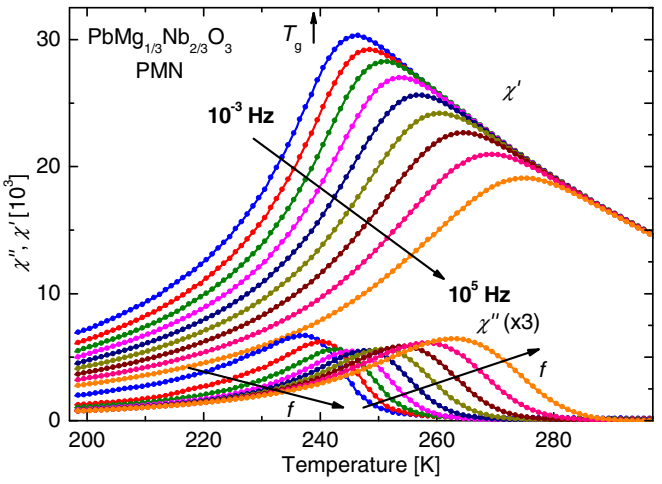

FIG. 2. Temperature dependencies of the dielectric susceptibility components χ' and χ'' of PMN at decade stepped frequencies within $10^{-3} \leqslant f \leqslant 10^{5}$ Hz. $T_g = 238.8$ K is marked by an arrow.

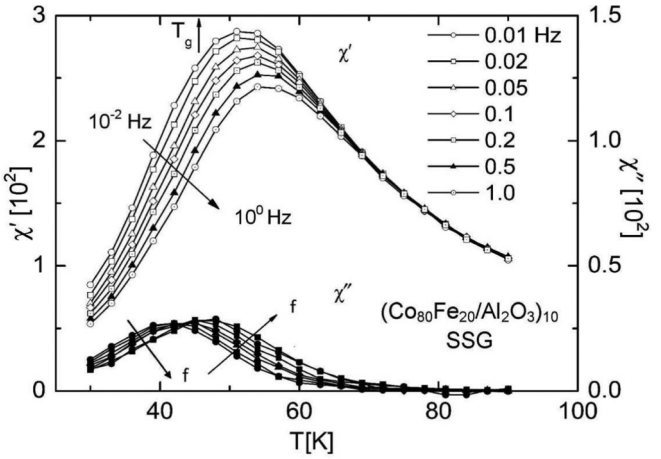

FIG. 3. Temperature dependencies of the magnetic susceptibility components χ' and χ'' of the superspin glass $[Co_{80}Fe_{20}(0.9\,nm)/Al_2O_3(3\,nm)]_{10}$ at decade stepped frequencies within $10^{-2} \leqslant f \leqslant 10^{0}$ Hz. $T_g = 45.6$ K is marked by an arrow. Reproduced with permission from [12].

Satisfactory agreement is also found for our magnetic SSG (Fig. 4; left data set), $z\nu = 10.2 \pm 4.6$ [18], while the low values of glass temperature, $T_g = (45.6 \pm 4.6)$K, and the large attempt time, $\tau_0 = (2.8 \pm 1.3) \times 10^{-7}$ s, are consequences of the relatively low density of the superspins [Fig. 1(a)] and their intrinsic activated dynamics, respectively [12].

Slightly above the critical region of PMN, $T/T_g > 1.03$ (Fig. 4; right dataset), the dynamics of the cluster system can no longer be described by Eq. (1). Obviously the

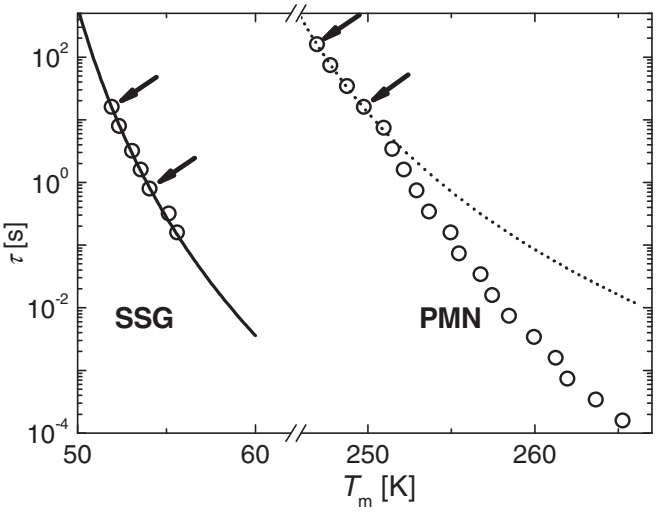

FIG. 4. Low-frequency relaxation times $\tau = (2\pi f)^{-1}$ vs peak temperatures $T_m(f)$ of χ' of PMN (Fig. 2) and SSG $[Co_{80}Fe_{20}(0.9\,nm)/Al_2O_3(3\,nm)]_{10}$ (Fig. 3) best-fitted to Eq. (1) (lines).

"superparaelectric" regime [19] is entered, where virtually noninteracting electric "supermoments" correspond to single PNRs and give rise to local polarization and giant susceptibility with large frequency dispersion. This "Vogel-Fulcher (VF) regime" is often described by a relaxation time corresponding to the cusp temperature T_m of $\chi'(f,T)$ [20],

$$\tau_{\rm VF}(T_m) = \tau_{\rm VF}^0 \exp[E_0/(T_m - T_{\rm VF})]. \quad (2)$$

Although satisfactory fits do exist for PMN, e.g., at frequencies within $10^2 \leqslant f \leqslant 10^5$ Hz [21], the significance of the emerging parameters $\tau_{\rm VF}^0$, E_0, and $T_{\rm VF}$ is ambiguous. Unlike the glass temperature T_g in Eq. (1) the interpretation of $T_{\rm VF}$ as a glassy "freezing temperature" is denied by theory [20]. We therefore abstain from further discussing the VF approach here and prefer the direct modeling of the interaction-free superparaelectric permittivity as proposed by Lu and Calvarin [22]. Their simulations of the dielectric response of $(PMN)_{0.95}(PbTiO_3)_{0.05}$ (PMN-PT, for short; see Fig. 13 in [22]) agree qualitatively with our χ' data shown in Figs. 2 and 3. This corroborates the absence of a phase transition within the underlying interaction-free approach.

IV. NONERGODICITY IN THE SUPERGLASS PHASES

Another indispensable property of a genuine glass phase is its nonergodicity, which has routinely to be checked at spin and dipolar glasses [13,14]. Figure 5 shows the standard procedure, which proves that the glass phase is thermally out of equilibrium except after being "aged" for a sufficiently long time at constant temperature. This is done here after continuously cooling the PMN sample from 240 to $T_a = 225$ K (curve 1) within 4.5×10^3 s followed by a halt at T_a of $\Delta t = 2.5 \times 10^5$ s (line 2). As a result the most sensitive quantity, χ''/χ', is found to decrease by ≈20% when approaching equilibrium by mere waiting. Peculiarly, further cooling to

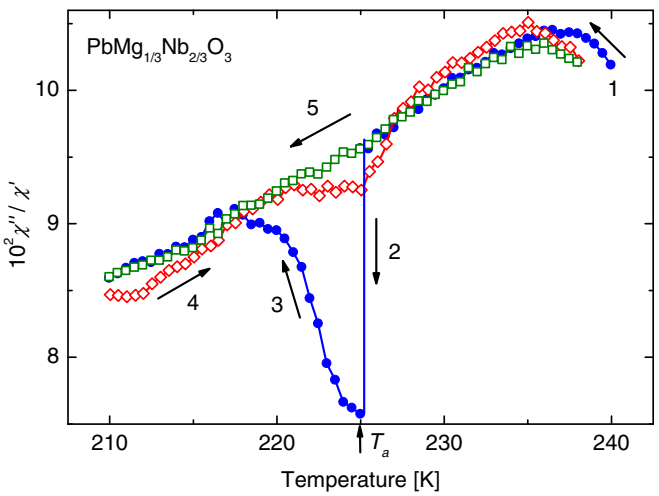

FIG. 5. Aging, rejuvenation, and memory of the susceptibility component ratio χ''/χ' of PMN measured vs T after ZFC from $T = 240$ K at rate $dT/dt = \pm 0.003\,{\rm K\,s^{-1}}$ and frequency $f = 0.1$ Hz on first cooling to 210 K with intermittent halt ($\Delta t = 2.5 \times 10^3$ s) at $T_a = 225$ K (curves 1–3), continuous reheating via memorized dip at T_a to 238 K (curve 4), and continuous cooling back to 210 K (curve 5).

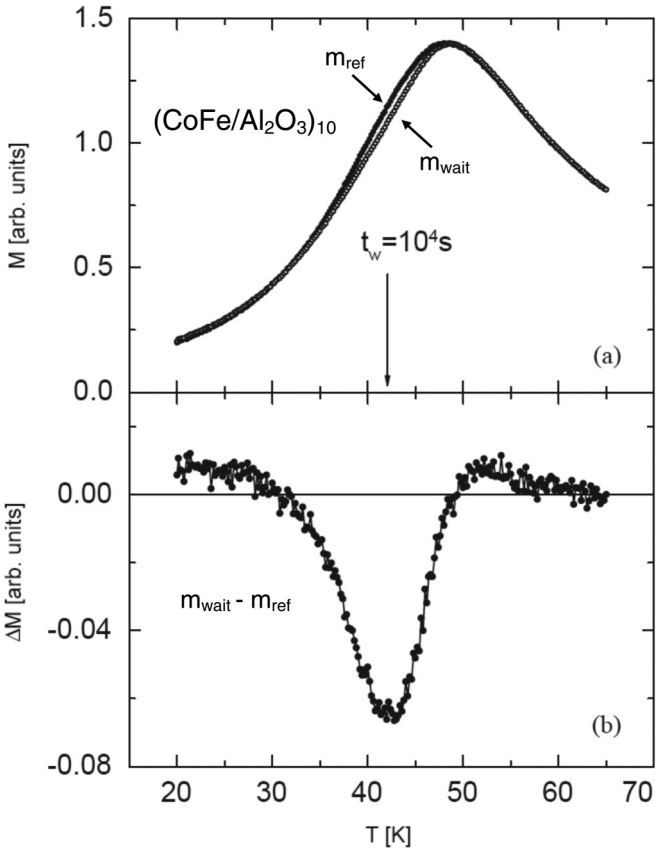

FIG. 6. Aging and rejuvenation of the magnetization $M(T)$ measured in $\mu_0 H = 40\,\mu$T in the SSG $[Co_{80}Fe_{20}(0.9\,{\rm nm})/Al_2O_3(3\,{\rm nm})]_{10}$: (a) Temperature dependencies of continuously measured $M_{\rm ref}(T)$ (solid circles) and of $M_{\rm wait}(T)$ (open circles) measured with intermittent zero-field wait period of $\Delta t = 10^4$ s at $T = 42$ K. (b) Magnetic hole $\Delta M = M_{\rm wait}(T) - M_{\rm ref}(T)$ vs T. Reproduced with permission from [23] via *CCC Rights Link*.

$T = 210$ K at the same rate yields a strong upward trend into the unaged curve ("rejuvenation" in curve 3), which is subsequently reproduced on continuously heating up to $T = 238$ K (curve 4) and recooling to $T = 210$ K (curve 5). At closer inspection, however, a dip of about 20% of the initial "dielectric hole" is recovered around T_a during heating (curve 4). This is attributed to the "memory" of the near-ground state being approached at T_a during the first extensive aging procedure.

A similar protocol is applied to test the SSG sample in Fig. 6 [23]. It illustrates the memory and rejuvenation effects of the zero-field-cooled dc magnetization in a field of 40 μT after a stop-and-wait procedure at $T_a = 42\,{\rm K} (= 0.95 T_g)$ for a duration $\Delta t = 10^4$ s. As seen in Fig. 6(a), the data corresponding to the intermittent stop-and-wait protocol, $m_{\rm wait}(T)$ (open circles), drop significantly below the reference curve, $m_{\rm ref}(T)$ (solid circles) at temperatures close to T_a. As seen in Fig. 6(b), the difference of the two data sets $\Delta m = m_{\rm wait}(T) - m_{\rm ref}(T)$ minimizes at T_a. This indicates that the magnetic moment configuration spontaneously rearranges toward equilibrium via growth of domains when the system is aged at T_a. These equilibrated domains become frozen-in on

further cooling and are retrieved on reheating. In other words, the system shows the memory effect.

The fact that $m_{\rm ref}(T)$ and $m_{\rm wait}(T)$ curves coalesce at low temperatures and only start to deviate as T_a is approached again from below clearly indicates that rejuvenation occurs as the temperature is decreased away from T_a in the stop-and-wait protocol. Rejuvenation is generally accepted as a strong hint at the chaotic nature of the glassy state.

V. FEATURES OF SSG AND PMN, RESPECTIVELY, AT THE SUPERGLASS TRANSITIONS

The $\chi''(T)$ curves in Figs. 2 and 3, respectively, resemble each other on a large scale, but differ in two respects from their $\chi'(T)$ counterparts. Their peak heights, $\chi''(T_m)$, are one order of magnitude lower and reveal conspicuous nonmonotonicities in their T dependencies. As indicated by arrows in Fig. 2 (bottom) and Fig. 3 (bottom) two temperature regimes differ by their cusp sequences below and above "inversion" temperatures $T_i \approx 245$ and 45 K, respectively: $\chi''(T_m)$ decreases at $T < T_i$ with increasing f, while it ascends at $T > T_i$ (arrows).

On PMN this peculiarity was observed by Colla *et al.* [24], but remained uncommented. Below we show that this spectral inversion indicates the onset of cluster glassy interaction as conjectured previously. Adequate indicators to this end are Cole-Cole (CC) plots of χ'' vs χ' [25] as shown in Figs. 7 and 8. Although these data are related to Figs. 2 and 3, they were measured separately for the sake of noise minimization along frequency scanned isotherms at discontinuously lowered ($\Delta T = -2$ to -5 K) temperatures $285 \geq T \geq 220$ K for PMN and $60 \geq T \geq 30$ K for the SSG. In the latter case an enhanced

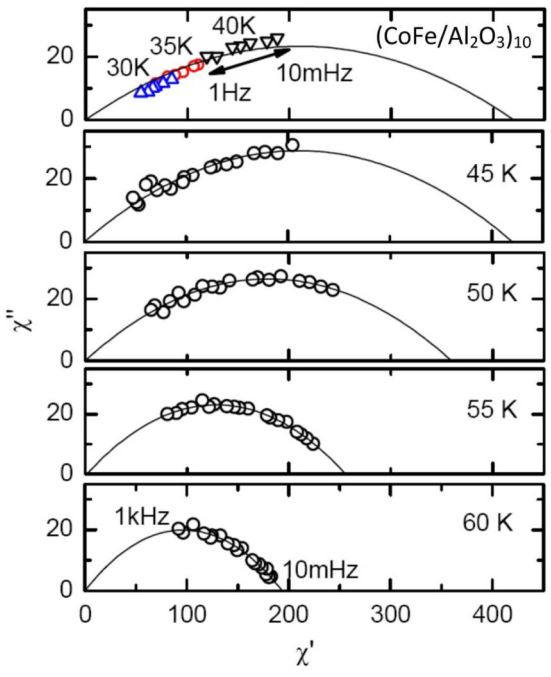

FIG. 7. Cole-Cole plots χ'' vs χ' of DMIM $[Co_{80}Fe_{20}(0.9\,\text{nm})/Al_2O_3(3\,\text{nm})]_{10}$ measured at $T = 30$, 35, 40 K within $10^{-2} \leqslant f \leqslant 10^{0}$ Hz, and at $T = 45$, 50, 55, and 60 K within $10^{-2} \leqslant f \leqslant 10^{3}$ Hz. Reproduced with permission from [12].

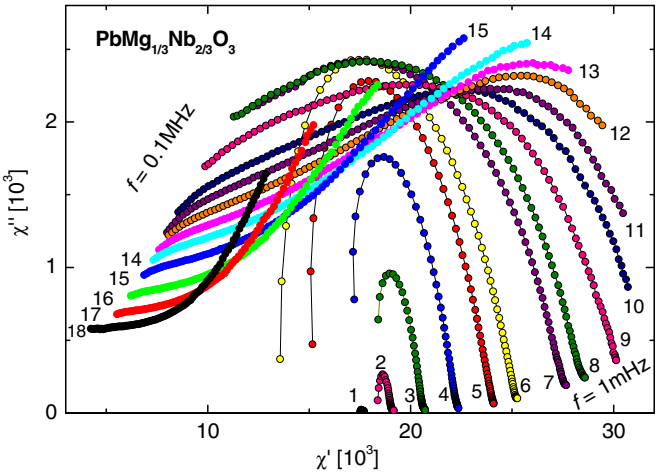

FIG. 8. Cole-Cole plots χ'' vs χ' of PMN measured at $T =$ 285(1), 280 (2), 275 (3), 270 (4), 265 (5), 262 (6), 256 (7), 254 (8), 250 (9), 246 (10), 244 (11), 242 (12), 240 (13), 238 (14) 235 (15), 230 (16), 225 (17), and 220 K (18) within $10^{-3} \leqslant f \leqslant 10^{5}$ Hz.

frequency range, $10^{-2} \leqslant f \leqslant 10^{3}$ Hz has been chosen for $T > 40$ K [26].

In the case of the SSG (Fig. 7) the CC plots are all truncated semicirclelike and are readily described by the Cole-Cole equation [27],

$$\chi(\omega) = \chi_s + (\chi_0 - \chi_s)/[1 + (i\omega\tau_c)^{1-\alpha}], \qquad (3)$$

where the correction exponent, $0 < \alpha \leq 1$, describes the degree of polydispersivity as distinguished from the monodisperse Debye process, $\alpha = 0$. As discussed previously [26], α is increasing from 0.75 to 0.87 as T decreases from 60 to 45 K, while it does not increase any more for $T \leq 40$ K (uppermost panel). This is a signature of the frozen glass state as $T < T_g \approx 44$ K. It is noticed that on decreasing T, the limited range of frequencies makes the data point groups continuously shift away from the rightmost intersection with the χ' axis, $\omega = 0$. Indeed, the fits [26] reflect the tremendous slowing down on cooling to the glass transition with "characteristic" relaxation times $10^{-4} \leqslant \tau_c \leqslant 10^{4}$ s at the apex points, $\omega\tau_c = 1$.

While the CC plots of the SSG clearly reflect the structural invariance of the cluster system (Fig. 1) under cooling to below the glass temperature, the situation changes fundamentally in the case of the relaxor, PMN. In Fig. 8 two drastically different groups of CC plots are clearly discernible in distinct temperature regions: (i) CC semicirclelike features dominate within $285 \geq T \geq 246$ K (curves 1–11), while (ii) "hockey stick"-like curves with horizontal "blade" and oblique "shaft" point to the high- and low-f directions, respectively, within $220 \leq T \leq 235$ K (curves 18–15), respectively. In the intermediate temperature range, $242 \geq T \geq 238$ K, the CC curves 12–14 undergo the drastic transformation from CC semicircles to the final hockey sticks.

Obviously the relaxing elements in the relaxor compound undergo a fundamental reorganization in the intermediate temperature range. On one hand they are closely linked to the phase transition from superparaelectric disorder into the superglassy state. On the other hand, and probably even more significant, a fundamental structural event takes place,

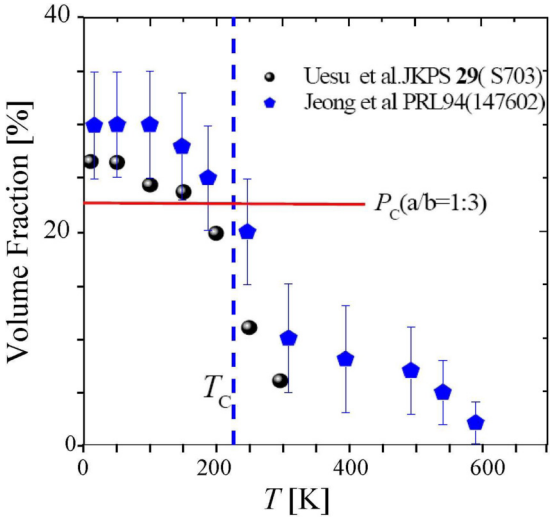

FIG. 9. Volume fraction of PNR in PMN estimated from neutron-scattering data (circular [28] and pentagonal dots [16], respectively). Lines are marking the conjectured percolation transition for elliptical shape at 23% [29] and $T_c \approx 230$ K [41], respectively. Adapted by permission from [30] via *Creative Commons License*.

viz. percolation of the continuously growing PNR under the control of electric RFs due to the still active cationic $Mg^{+2} - Nb^{5+}$ charge disorder. Neutron scattering data (Fig. 9) have evidenced [28,29] that the volume fraction of PNR in PMN is overcoming the percolation threshold of 23% for the elliptical shape [29] at a conjectured ferroelectric phase transition at $T_c \approx 230$ K [30]. This opens the chance to form large coherent ferroelectric domains, whose dynamic phenomenology strongly reminds one of domain-wall (DW) dynamics in disordered ferroics represented by CC diagrams in the complex permittivity plane [31,32].

Let us first consider the superparaelectric region of PMN at high-T, $285 \geq T \geq 246$ K (Fig. 8, curves 1–11). A similar extreme "blowing up" of the superparaelectric CC curve from a "dot" (285 K) to a gigantically broad distribution (246 K) was reported previously [33]. Axial ratios $\Delta\chi'/2\Delta\chi'' \approx 2.5$ and 6 at 275 and 250 K, respectively, are found and strongly exceed unity of a monodispersive Debye relaxator. Our accessible spectral range does not suffice to correctly determine the width of the CC semicircles at $T < 246$ K, where recording of the very low-f branch would require submillihertz driving fields.

Another extraordinary [33] observation is the skewness of the CC plots and its temperature dependence. It starts with positive sign (i.e., peaking at the high-f side) within $285 \geq T \geq 262$ K (curves 1–6), passes through a "crossover" regime within $256 \geq T > 254$ K (curves 7–8), and ends up negatively (i.e., peaking at the low-f side) within $250 \geq T \geq 246$ K (curves 9–11). Positive skewness is well known from polydispersive polar cluster systems such as $SrTiO_3$: Ca [34], as modeled in PMN-PT [22], and mathematically described with a Lacroix-Béné-type [35] distribution of relaxation times, $\tau = (2\pi f)^{-1}$,

$$G(\tau) = [\sin(\pi\beta)/\pi][\tau_0/(\tau - \tau_0]^{\beta}, \quad \text{for } \tau > \tau_0, \qquad (4)$$

where $G(\tau) = 0$ for $\tau < \tau_0 =$ shortest relaxation time, and polydispersivity exponent $\beta \leqslant 1$. In the case of relaxor ferroelectrics it is found to match with an exponentially decreasing volume distribution of PNR, $N(V) \propto \exp[(V_m - V)/V_0]$, $V_m =$ minimum cluster size, $V_0 =$ width of size distribution [22]. It determines the distribution of cluster relaxation times via Arrhenius-type activation, $\tau = \tau_0 \exp(KV/k_BT)$, $\tau_0 =$ ionic attempt time, $K =$ anisotropy energy density, $k_B =$ Boltzmann constant. Within this theory the low-f tail of the CC "semicircle" is predicted to drop linearly under an angle $n\pi/2$, where the coefficient $n = k_BT/E_0$ decreases linearly with T. This subtle effect is confirmed for the asymptotic right-hand tails of curves 2–6 in Fig. 8, where n drops from 0.51 to 0.27 between $T = 280$ and 262 K. It implies both substantial broadening of the size distribution and growth of the PNR. Actually this result reinforces previous insight into PNR growth via quenched fluctuations of RFs in PMN-PT on cooling toward the glass temperatures [36].

The crossover to negative skewness (Fig. 8: curves 7–11) signifies the upcoming relevance of intercluster interaction within $256 \geq T \geq 246$ K, which is neglected by Lu and Calvarin [22]. It is indispensable for the freezing process of the percolating glassy cluster as $T \to T_g$ and highlights the preponderance of large clusters with steadily growing relaxation times. Polydispersive models labeled as Cole-Davidson [37] or Havriliak-Negami [38], both showing negative skewness, might be chosen to approximately describe the CC semicircles enclosing the glass temperature, $242 \geqslant T_g \geqslant 238$ K (Fig. 8: curves 12–14). Within this interval the glass transition is more accurately pinpointed by the divergence of the characteristic relaxation time related to the peak temperatures $T_m(f)$ of χ' via the critical power law, Eq. (1), as discussed in Sec. III.

While at $T > T_g$ the relaxor refers to fluctuating, hence mobile clusters, these become immobile and stick domainlike together at $T < T_g$ as a result of glassy freezing. All mobility under low external electric fields is now restricted to the interfaces between the clusters. These behave essentially like ferroic DWs under the constraint of pinning forces due to the still existing quenched electric RFs. In this situation a driving electric field will merely excite different modes of DW motion as observed in disordered ferroic materials such as periodically poled ferroelectric $KTiOPO_4$ [31]. They are described in terms of a "universal DW dynamics of disordered ferroics" [31,32] by CC diagrams in the complex permittivity plane:

(i) The essentially flat polydispersive relaxation response of oscillating DW segments as defined by a high density of pinning centers formally yields the CC equation, Eq. (2). Owing to the wide distribution of "Larkin lengths" between pinning centers the CC semicircles in PMN are essentially flat and result in a white-noise-like spectrum as e.g., also observed in the soft superferromagnetic discontinuous metal-insulator multilayer $[Co_{80}Fe_{20}(1.4\,\text{nm})/Al_2O_3(3\,\text{nm})]_{10}$ [39].

(ii) The creep regime describes the thermally activated net propagation of the DWs after overcoming the depinning threshold at very low frequencies, $\omega < \omega_p$,

$$\chi' - i\chi'' = \chi_\infty[1 + (i\omega\tau)^{-\delta}], \quad 0 < \delta < 1, \qquad (5)$$

which is readily transformed into the linear function $\chi''(\chi') = (\chi' - \chi_\infty)\tan(\delta\pi/2)$ as observed (Fig. 8). E.g., at $T = 220$ K and $\chi' \approx 7500$ the imaginary component starts rising from $\chi''(f_p \approx 10^2\,\text{Hz}) = 630$ to $\chi''(10^{-3}\,\text{Hz}) = 1640$. The slope of

this function results from scaling of the dynamical relaxation-to-creep transition of DWs [39] and yields $\delta = (2 - x)/z$, where the *fractality exponent* $x \geqslant 1$ represents the roughness of the interfacial (DW) contour line and z the *dynamical exponent*. E.g., from the experimental value $\delta(220\text{K}) \approx 0.45$ and $z = 1.56$ [40] the fractal dimension $x \approx 1.30$ of interfacial contour lines in glassy PMN is obtained. Upon approaching T_g the slope decreases to $\delta(238\,\text{K}) \approx 0.10$, hence, $x \approx 1.84$ characterizes utmost wall roughness preceding the total loss of cluster connectivity at $T \geqslant T_g$.

(iii) The transitions between the horizontal and inclined relaxation and creep lines, respectively, in Fig. 8 become more and more rounded as T increases. This phenomenon is well known, e.g., from periodically poled $KTiOPO_4$ [31], where the relaxation and the creep processes are controlled by distribution functions of local double-well potentials and DW mobilities, respectively. Since these are not identical by nature, their transition frequencies f_p cannot be identical at all temperatures and the dynamical transition will become smeared.

(iv) Finally, at still lower frequencies the dynamical transitions "creep-to-slide" and "slide-to-switching" are expected [32], but remain to be shown at much higher ac voltages.

At first glance the appearance of domain walls in the glassy state of PMN is surprising. However, one has, again, to take into account the action of quenched electric RFs in the charge disordered host material. They will become active at the percolation transition of the PNR occurring in the vicinity of the glass transition (Fig. 9). Since RFs are known to favor local mesoscopic order (via their statistical fluctuations), they are also expected to take care of maximizing polar partial volumes, *viz.* condensing nano- into microdomains as observed in recent low-T transmission electron micrographs [30]. Such a process was also conjectured from diffuse neutron-scattering experiments on PMN [41] and from quasielastic light-scattering data, which clearly hint at percolation of the polar nanoregions into a fractal with dimension $d_p \approx 2.6$ at $T_p \approx 240\,\text{K}$ [42].

An important, if not decisive ingredient of domain growth is finally the occurrence of a global lattice instability due to the softening of the ferroelectric F_{1u} lattice mode in PMN [43] around $T_p \approx T_g$. This feature and the observation of ferroelectric microdomains have been considered as signatures of a factual ferroelectric phase transition in PMN [30]. However, one has definitely to respect the undisputed existence of crucial cluster glass properties discussed above (Fig. 5) and to accept that the topography of the microdomain walls remains controlled by RFs [see Figs. 7(d) and 7(e) in [30]]. They eventually form what might be called a *super-superdipolar* glass ground state undergoing nonetheless standard criticality and nonergodicity.

VI. CONCLUSION

The concept of ferroic glasses comprising three kinds of mesoscopic glasses, *viz.* spin cluster glass, strain glass, and ferroelectric relaxors [8], appears appealing for a common qualitative understanding of their mesoscopic glass transitions. Here we have compared the formation and the properties of two superdipolar glasses consisting of ensembles of superparamagnetic nanoparticles in an insulating environment, $[Co_{80}Fe_{20}(0.9\,\text{nm})/Al_2O_3(3\,\text{nm})]_{10}$, and quasiferroelectric nanoregions (PNRs) in the paraelectric host crystal of PMN, respectively.

While the comparison of the dynamic critical behavior and the basic properties of nonergodicity makes no distinction between both samples, the intimate dependence of the PNR in PMN on the inherent quenched RFs introduces decisive anomalies at the genesis of the final superglass ground state:

(i) The creation and stabilization of initial PNRs is due to the instability of the polar soft mode of PMN and its driving of the local phase transition at T_d under the constraint of RF fluctuations.

(ii) Their subsequent growth up to the percolation limit on cooling is controlled by the RFs.

(iii) Coarse-graining into a ferroelectric microdomain landscape [30] mirrors the "ordering" process of the superglass under the control of RFs.

In conclusion, 25 years after the primordial statement of a "RF-induced domain state" in the relaxor PMN [3] we are returning to a related one, where the "domains" are now extending to mesoscopic size. While previously the mere breaking of long-range order into nanodomains had been accepted according to the original theory of RF magnetism [44], we are now acknowledging a subsequent glass formation via mutual interaction of the primary domains. The action of electric RFs helps finally building the superdomain ground state of PMN coming close to a "ferroelectric with multiple inhomogeneities" [45].

ACKNOWLEDGMENTS

We are grateful to S. Sahoo for providing the DMIM data of Figs. 3 and 7 [12]. Work at Katowice was supported by the Polish Ministry of Science and Higher Education under the project "Magnetic and ferroelectric multifunctional materials for electronics."

[1] G. A. Smolenskii and A. I. Agranovskaya, Sov. Phys. Tech. Phys. **3**, 1380 (1958).
[2] D. Viehland, J. F. Li, S. J. Jang, L. E. Cross, and M. Wuttig, Phys. Rev. B **43**, 8316 (1991).
[3] V. Westphal, W. Kleemann, and M. D. Glinchuk, Phys. Rev. Lett. **68**, 847 (1992).
[4] W. Kleemann, J. Dec, R. Blinc, B. Zalar, and R. Pankrath, Ferroelectrics **267**, 157 (2002).
[5] A. A. Bokov and Z.-G. Ye, J. Mater. Sci. **41**, 31 (2006).
[6] N. Novak, R. Pirc, M. Wencka, and Z. Kutnjak, Phys. Rev. Lett. **109**, 037601 (2012).

[7] W. Kleemann, J. Dec, and S. Miga, Phys. Status Solidi B **251**, 1993 (2014).

[8] X.-B. Ren, Phys. Status Solidi B **251**, 1982 (2014).

[9] C. W. Ahn, C.-H. Hong, B.-Y. Choi, H.-P. Kim, H.-S. Han, Y. H. Hwang, W. Jo, K. Wang, J.-F. Li, J.-S. Lee, and I. W. Kim, J. Kor. Phys. Soc. **68**, 1481 (2016).

[10] S. Sahoo, O. Petracic, W. Kleemann, S. Stappert, G. Dumpich, P. Nordblad, S. Cardoso, and P. P. Freitas, Appl. Phys. Lett. **82**, 4116 (2003).

[11] In addition to the "microscopic" RFs due to the statistical charge disorder of Mg^{2+} and Nb^{5+} ions in the *B*-site cation sublattice, these cations form also one-by-one ordered clusters in PMN. These electrically charged "chemically ordered regions" (CORs) provide additional coarse-grained RFs, but are not expected to provide basically new physics [3].

[12] S. Sahoo, Ph.D. thesis, University Duisburg-Essen, 2003.

[13] K. Binder and J. D. Reger, Adv. Phys. **41**, 547 (1992).

[14] K. Binder and A. P. Young, Rev. Mod. Phys. **58**, 801 (1996).

[15] A. T. Ogielski, Phys. Rev. B **32**, 7384 (1985).

[16] I. K. Jeong, T. W. Darling, J. K. Lee, T. Proffen, R. H. Heffner, J. S. Park, K. S. Hong, W. Dmowski, and T. Egami, Phys. Rev. Lett. **94**, 147602 (2005).

[17] J. A. Quilliam, S. Meng, C. G. A. Mugford, and J. B. Kycia, Phys. Rev. Lett. **101**, 187204 (2008).

[18] S. Sahoo, O. Petracic, Ch. Binek, W. Kleemann, J. B. Sousa, S. Cardoso, and P. P. Freitas, Phys. Rev. B **65**, 134406 (2002).

[19] L. E. Cross, Ferroelectrics **76**, 241 (1987).

[20] A. K. Tagantsev, Phys. Rev. Lett. **72**, 1100 (1994).

[21] D. Viehland, S. L. Jang, L. E. Cross, and M. Wuttig, J. Appl. Phys. **68**, 2916 (1990).

[22] Z. G. Lu and G. Calvarin, Phys. Rev. B **51**, 2694 (1995).

[23] S. Sahoo, O. Petracic, W. Kleemann, P. Nordblad, S. Cardoso, and P. P. Freitas, J. Magn. Magn. Mater. **272–276**, 1316 (2004).

[24] E. V. Colla, E. Yu. Koroleva, N. M. Okuneva, and S. B. Vakhrushev, J. Phys.: Condens. Matter **4**, 3671 (1992).

[25] K. S. Cole and R. H. Cole, J. Chem. Phys. **9**, 341 (1941).

[26] O. Petracic, S. Sahoo, Ch. Binek, W. Kleemann, J. B. Sousa, S. Cardoso, and P. P. Freitas, Phase Transit. **76**, 367 (2003).

[27] A. K. Jonscher, *Dielectric Relaxation in Solids* (Chelsea Dielectrics, London, 1983).

[28] Y. Uesu, H. Tazawa, K. Fujishiro, and Y. Yamada, J. Kor. Phys. Soc. **29**, S703 (1996).

[29] E. J. Garboczi, K. A. Snyder, J. F. Douglas, and M. F. Thorpe, Phys. Rev. E **52**, 819 (1995).

[30] D. Fu, H. Taniguchi, M. Itoh, and S. Mori, in *Advances in Ferroelectrics* (InTech Open Access Publ., Rijeka, 2012), Chap. 3, p. 51.

[31] T. Braun, W. Kleemann, J. Dec, and P. A. Thomas, Phys. Rev. Lett. **94**, 117601 (2005).

[32] W. Kleemann, Annu. Rev. Mater. Res. **37**, 415 (2007).

[33] A. Levstik, Z. Kutnjak, C. Filipic, and R. Pirc, Phys. Rev. B **57**, 11204 (1998).

[34] U. Bianchi, J. Dec, W. Kleemann, and J. G. Bednorz, Phys. Rev. B **51**, 8737 (1995).

[35] R. P. Lacroix and G. J. Béné, Arch. Sci. **4**, 430 (1951).

[36] V. V. Shvartsman, J. Dec, T. Łukasiewicz, A. L. Kholkin, and W. Kleemann, Ferroelectrics **373**, 77 (2008).

[37] D. W. Davidson and R. H. Cole, J. Chem. Phys. **18**, 1417 (1950).

[38] S. Havriliak and S. Negami, Polymer **8**, 161 (1967).

[39] X. Chen, O. Sichelschmidt, W. Kleemann, O. Petracic, Ch. Binek, J. B. Sousa, S. Cardoso, and P. P. Freitas, Phys. Rev. Lett. **89**, 137203 (2002).

[40] T. Nattermann, V. Pokrovsky, and V. M. Vinokur, Phys. Rev. Lett. **87**, 197005 (2001).

[41] G. Xu, G. Shirane, J. R. D. Copley, and P. M. Gehring, Phys. Rev. B **69**, 064112 (2004).

[42] A. Koreeda, H. Taniguchi, S. Saikan, and M. Itoh, Phys. Rev. Lett. **109**, 197601 (2012).

[43] H. Taniguchi, M. Itoh, and D. Fu, J. Raman Spectrosc. **42**, 706 (2011).

[44] Y. Imry and S. K. Ma, Phys. Rev. Lett. **35**, 1399 (1975).

[45] D. Fu, H. Taniguchi, M. Itoh, S.-Y. Koshihara, N. Yamamoto, and S. Mori, Phys. Rev. Lett. **103**, 207601 (2009).